Journal of The Electrochemical Society

Characterization of the Interfaces in $LiFePO_4$/PEO-LiTFSI Composite Cathodes and to the Adjacent Layers

JES Focus Issue of Selected Papers from IMLB 2018

Characterization of the Interfaces in $LiFePO_4$/PEO-LiTFSI Composite Cathodes and to the Adjacent Layers

Verena Wurster,[1,2,z] Christine Engel,[1] Heiko Graebe,[1,3] Thimo Ferber,[2] Wolfram Jaegermann,[2] and René Hausbrand[2]

[1] *Robert Bosch GmbH, Corporate Sector Research and Advanced Engineering, 71272 Renningen, Germany*
[2] *Darmstadt University of Technology, Surface Science Division, 64287 Darmstadt, Germany*
[3] *Insitute for Particle Technology, TU Braunschweig, 38104 Braunschweig, Germany*

Interface resistances between the different components of battery cells limit their fast charge and discharge capability which is required for different applications such as electromobility. To decrease interface resistances, it is necessary to understand which individual interface they arise at and how they can be controlled. Electrochemical impedance spectroscopy is a well-established technique for the distinction of different contributions to the internal cell resistance and allows the characterization of interface resistances. Especially the use of suitable cell setups allows one to attribute the measured resistances to specific interfaces. In this contribution, we investigate the impedance of dry polymer full cells containing a lithium iron phosphate/ poly(ethylene oxide)-lithium bis(trifluoromethanesulfonyl)imide composite cathode, a solid polymer electrolyte separator and a lithium-metal anode. Based on the results on different cell setups, we are able to reliably determine the planar resistances between the components as well as the charge transfer resistance inside the composite cathode. For unoptimized systems, we find high planar resistances, which can be significantly reduced by coating and processing strategies. For the charge transfer resistance, we find a dependence on the SOC as well as on the charging direction. Possible mechanisms for the evolution of interface resistances are discussed also based on chemical analysis performed by photoelectron spectroscopy (XPS).

 [DOI: 10.1149/2.0621903jes]

Manuscript submitted October 26, 2018; revised manuscript received January 9, 2019. Published January 23, 2019. *This paper is part of the JES Focus Issue of Selected Papers from IMLB 2018.*

Solid-state lithium batteries are a promising future battery technology. They offer the potential to reach higher energy densities and could be a safer alternative to batteries with liquid electrolyte.[1–3] Dry solid polymer electrolytes (SPE) offer a high safety, flexibility and durability.[3,4] Due to their low ionic conductivity, they require a high operation temperature of 80°C.[5]

Due to the mechanical properties of the used solid polymer electrolyte, the application of lithium metal as an anode is possible. This results in a highly increased energy density. Therefore, the full cells in this work are corresponding to half-cells in standard lithium-ion cells.

A key requirement for battery cells for automotive applications is the fast-charge and fast-discharge capability. Therefore, low interface resistances in the complete cell are important. In this regard, as solid-state batteries suffer from poor connections between the different materials, this means that in general they are inferior to those in batteries with liquid electrolyte.

As the battery cell contains different components, the resistances between them hinder the lithium ion and electron transport through the cell. Figure 1 shows the setup of a full cell containing a composite cathode with a current collector, a solid polymer electrolyte membrane (SPE) and a lithium anode schematically. The composite cathode consists of cathode active material (CAM), carbon additive and the catholyte, which typically consists of a similar solid polymer as in the SPE. All the existing interfaces are marked. Also shown are the pathways for the Li^+-ions and electrons, which lead through several bulk materials and interfaces. Low resistances for these charge carriers in the bulk materials and at the interfaces are important for achieving high capacities also at high C-rates. In order to distinguish between bulk and interface resistances and to assess how the resistances are distributed to the several interfaces, a detailed electrochemical analysis is required which can be carried out by electrochemical impedance spectroscopy (EIS) using different types of cells.

Electrochemical impedance spectroscopy (EIS) is a well-established technique for the characterization of interface resistances. An electrochemical impedance spectrum of a full cell contains contributions from all parts of the cell. These are in particular the electrolyte bulk resistance, the resistances between the layers of the different components such as between SPE-membrane and composite electrode or between composite electrode and current collector, as well as the resistance between the CAM and the catholyte in the composite cathode. While the resistance between the components are related to the geometric area, i.e. they are planar interface resistances, the resistance between CAM and catholyte depends on the total contact area between these two phases in the composite electrode.

Most often impedance spectra are displayed in the Nyquist plot, where the imaginary part of the impedance is plotted against the real part as a function of frequency. Spectra of cells which have two planar interface resistances, and at least one composite electrode, can be modelled by an electrical analogy consisting of an equivalent circuit model as shown in Figure 2. Here an exemplary full cell spectrum in the initial state is displayed, as well as the fit curve of the full cell, and the fit curves of the individual parts.

For a solid polymer based battery, the serial resistance (R_{serial}), seen as the x-interception at high frequencies, represents the ionic resistance of the SPE layer, which depends on its ionic conductivity and thickness. The semicircle contributions in the high and middle frequency region are caused by planar interfaces resistances, which may be resistances either for ion or electron transfer depending on the type of the interface (R_{if}). The shape of the curve at low frequencies is due to the composite nature of the electrode, and can be modelled by a transmission line model (TLM). This model for describing the impedance of composite cathodes was first introduced by Euler and Nonnenmacher.[6] To describe the very low frequencies, a Warburg open element is connected in series to the TLM. It is typically related to diffusion of Li^+- ions in the electrolyte.[7] Furthermore diffusion of Li^+- ions inside the active material can contribute to this Warburg element.

A typical TLM is shown in Figure 3. This consists of electronic resistances in the electrode (r_{el}), ionic resistances in the catholyte (r_{ion}) and R-CPE elements representing the interface between CAM and catholyte. The resistance for Li^+-ion transfer at the CAM-catholyte interface is typically called charge transfer resistance (R_{ct}), and is proportionate to the surface of the CAM.

[z] E-mail: Verena.haerdtner@de.bosch.com

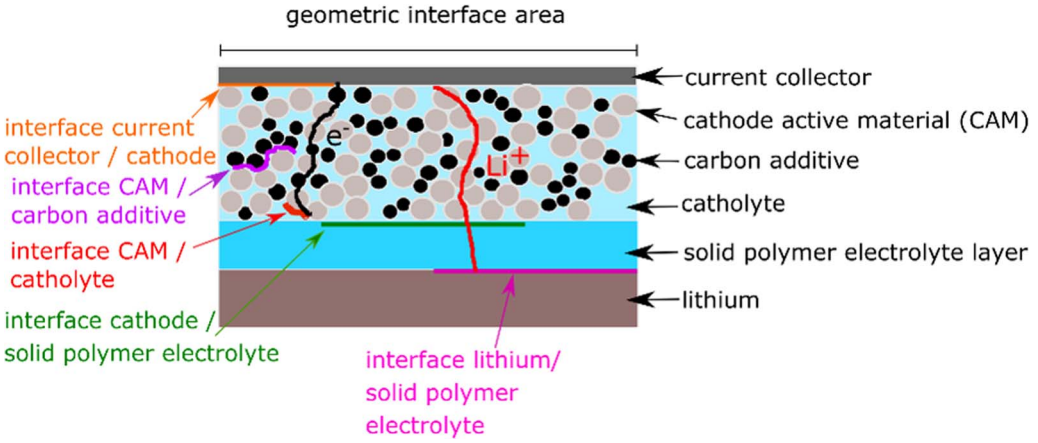

Figure 1. Schematic figure of a lithium polymer cell with a composite cathode and a lithium metal anode. The different interfaces are marked.

Since the charge transfer appears on each LFP particle surface (pore), through the whole cathode, the total R_{CT} results from the many particular r_{CT} occurring at these pores. The ionic and electronic resistances are also separable into the parts r_{el} and r_{ion} at each pore, adding these up and multiplying with the pore number n gives the total resistances R_{el} and R_{ion}. For modelling a fictive pore number of $n = 100$ was used.

Impedance spectra are often difficult to evaluate because the different processes cannot be clearly distinguished. The extent to which the different features in the impedance spectra are separated depends on the characteristic frequency f_{max}, which is related to the interface capacitance (C) and resistance (R) according to

$$2\pi f_{max} \cdot R \cdot C = 1 \qquad [1]$$

According to Irvine et al.[8] an area specific capacitance in the region of 10^{-6} F/cm^2 is typical for an interface. If the resistances on the interfaces show similar values and their area is the same, which is often the case for planar resistances, the respective half cycles in the impedance spectra appear at similar frequencies and strongly overlap. On the other hand, if the area is a lot larger than the geometric surface area, as it is for the interface between the CAM and the catholyte, the impedance is expected at lower frequencies. Therefore, the absolute capacitance is magnitudes higher and the absolute resistance should be in the same order of magnitude compared to the planar resistances. This means, that the area specific resistance is orders of magnitudes higher for the charge transfer resistance. Since on this interface, an insertion reaction takes place, involving the Li^+-ions and electrons, a high area specific resistance is expected.

For standard full cells, an overlap of the different interface resistances in the impedance spectrum is almost inevitable. Therefore, the assembly of specific cell configurations is required to understand the complete impedance response of a cell. The separate analysis of the interface resistances on the anode and the cathode side is possible by the use of symmetric cells with either two cathodes or two lithium anodes. In addition, the ionic conductivity of the SPE and the electronic conductivity of the composite electrode may be independently determined using blocking electrodes.

In the symmetric cells, the electrodes are only characterized in the initial state. In this state, the majority of CAM show an electrical blocking behavior. Therefore no charge transfer reaction takes place.[4,9]

A certain state of charge (SOC) can be adjusted in full cells. However, there is an overlay of the cathode impedance with the impedance of the lithium side.

An approach for measuring the cathode EIS at different SOC, known from the analysis of cells with liquid electrolyte,[10,11] is to disassemble two full cells with a defined SOC and to reassemble the cathodes in a cathode symmetric cell. Up to now, it was not possible to properly disassemble charged full cells, built up with polymer electrolyte, due to the high adhesion of the polymer electrolyte based layers.

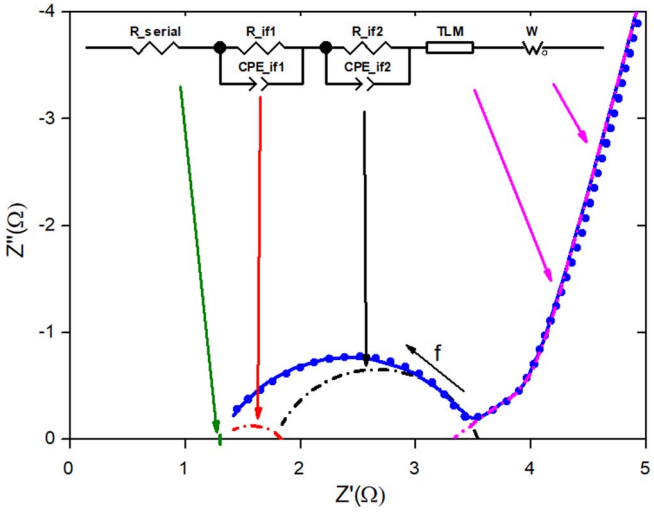

Figure 2. Exemplary EIS spectrum of a full cell in the Nyquist plot (blue points) and the corresponding fit (blue line). The equivalent circuit which was used for fitting is displayed in the insert. It consists of a serial resistance for the electrolyte bulk phase, (R_{serial}), two R-CPE elements representing two planar interface resistances, a transmission line (TLM) for a porous (or composite) electrode and a Warburg element (W). All the separate components of the fit are displayed.

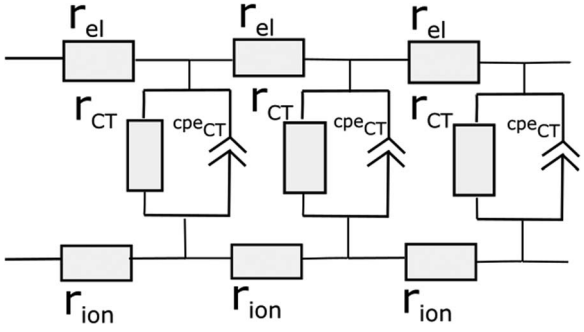

Figure 3. Equivalent circuit of the transmission line model describing the different contributions in a composite cathode. In this figure n, the number of elements, representing the number of interfaces, is 3, for fitting $n = 100$ was used.

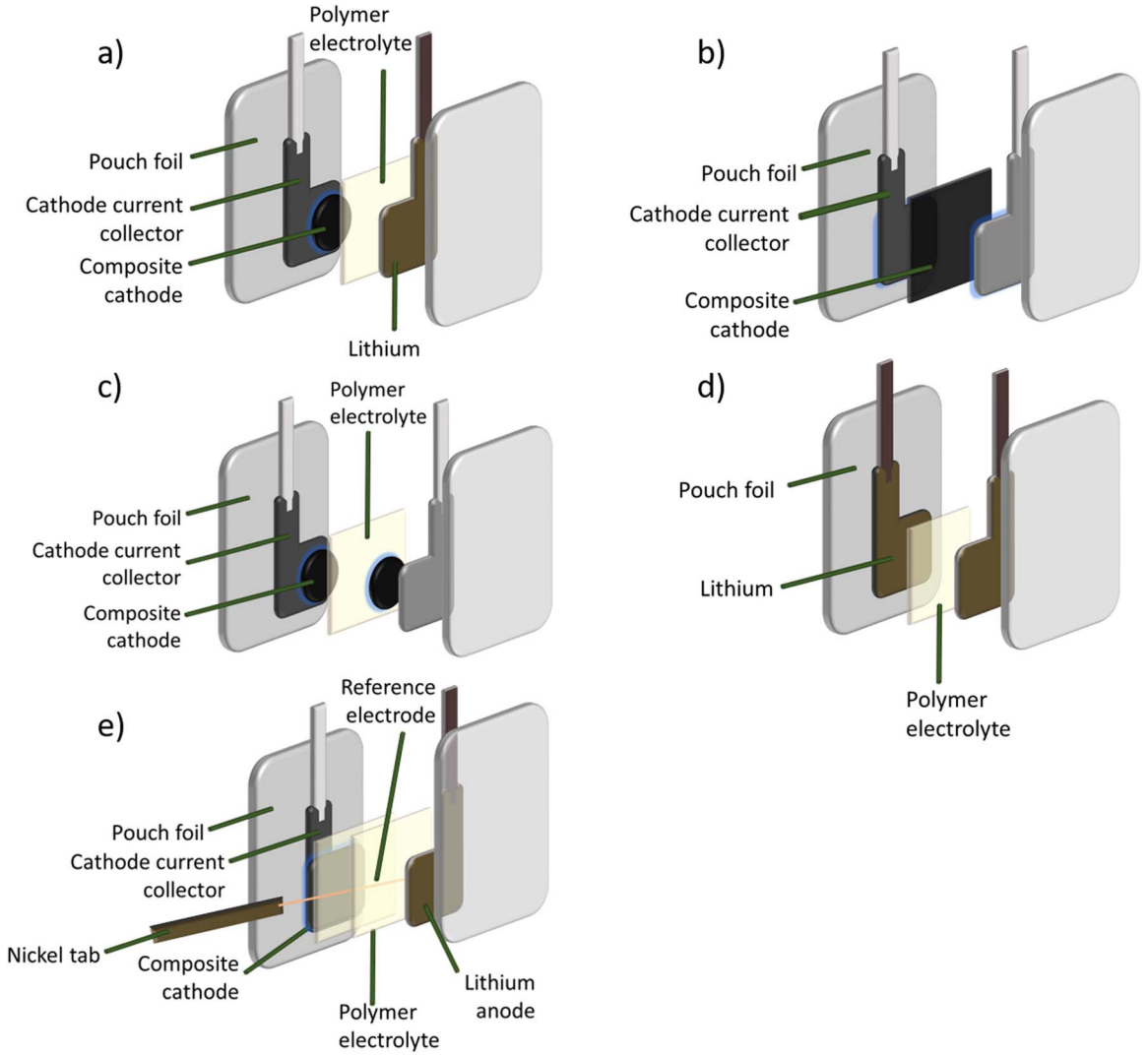

Figure 4. Schematic setup of a full cell (a), a cathode sandwiched between two current collectors (b), a cathode symmetric cell (c), a lithium symmetric cell (d) and a full cell with a reference electrode (e).

Cells with a reference electrode (Figure 4e) enable the separation of the cathode and the anode spectra in a working full cell. These full cells can be charged and discharged, so the cathode spectra of different SOC are measured in situ.

This work investigates the resistance contributions of poly(ethylene oxide) (PEO)-based solid electrolyte full cells with a Li_xFePO_4 (LFP) composite cathode and a planar Li-metal anode using EIS analysis on full and symmetric cells.

The focus of the research is the charge transfer resistance between the catholyte and LFP, which is also investigated at different state of charge using a reference electrode. As conductive salt in the SPE and the catholyte, lithium bis(trifluoromethanesulfonyl)imide (LiTFSI) in a ratio of $[Li^+]:[EO] = 1:10$, was applied; carbon black was used to improve the electronic conductivity in the cathode composite.

LFP is an attractive material for PEO based cells because its cutoff voltage of 3.6 V lies within the stability window of PEO, which is unstable at potentials above 3.8 V.[2,12] It is also environmentally friendly, low priced and has a high capacity of 170 mAh/g.[13,14] Although it is an established and well-characterized material, there are diverse theories about the single-particle lithiation mechanism in LFP and its consequences on charge transfer resistance.[15] Padhi et al.[14] claimed a two-phase interface between a region consisting of pure LFP and a completely delithiated region of pure $FePO_4$ (FP) existing in a single particle. This interface would hinder the charge and discharge kinetics and as a result, they supposed LFP would only suit for low rate applications. Since high charge- and discharge rates are possible in LFP cathodes, there are many critics on this model and many alternative theories.[15] Concerning the charge transfer resistance in a LFP/ PEO-LiTFSI composite cathode, there are only few publications. Hanai et al.[16] characterized partly charged cathodes by building up cathode symmetric cells and charging them by a stainless steel mesh. This mesh is placed between two polymer electrolyte layers, comparable to the reference electrode in our study. This cell setup enabled a charge of the cathodes until $Li_{0.6}FePO_4$ (SOC 40) by Li deposition on the mesh at 50°C. By fitting the low frequency region by means of an R-C element, they determined a decreasing charge transfer resistance during charge until SOC 40 and a reversible increase during discharge.

Experimental

Cathode processing.—A solvent-free preparation technique introduced by Graebe et al.[17] was applied for the composite cathodes characterized in this work. This technique offers a wider range of advantages compared to the typically used solvent-based processing (for example applied by Hanai et al.[18] for this material system). The solvent-free process is supposed to be more cost-efficient since it has less processing steps. Since there is no hazardous solvent used, the dry

Table I. Ratio of materials in the characterized composite cathodes. Information in wt%.

LFP	PEO	LiTFSI	Carbon black
66,8	18,0	11,8	3,4

processing is environmental friendlier and no impurities of residual solvent and water are brought into the cell.[17]

All the used materials being part of the composite cathode, which are in particular PEO ($M_v = 600000$; Sigma Aldrich), LiTFSI (Sigma Aldrich), LFP (carbon coated, Life Power P2, Clariant) and carbon black (Timcal Super C 65), were dried under vacuum before usage. The preparation was done in an argon-filled glove box ($H_2O < 1$ ppm, $O_2 < 1$ ppm, MBraun). Therein, the cathode components were weighted in quantities corresponding to the target composition as stated in Table I and mixed using a dual asymmetric centrifugal mixer. The mixed powder was pressed, resulting in a cathode pellet, by the usage of a pressing die heated up to 80°C. The mixing and powder pressing was carried out according to Graebe et al.[17] After pressing, the pellets were calendered at 90°C to a final thickness of either 40 µm or 100 µm. From the resulting freestanding cathode sheets, cathode pieces with a defined surface area were punched out.

Cell assembly.—Using these cathodes, pouch cells with different designs were assembled as displayed in Figure 4.

The cells in Figures 4a–4d were built up in an argon-filled glove box. Standard full cells (Figure 4a) were built up by using an aluminum current collector, a cathode (Ø 16 mm), an inhouse processed SPE (50 µm thickness) and a 60 µm thick lithium foil anode (A = 5.45 cm^2, Honjo chemical corporation). A nickel tab was used as current collector on the anode side. After stacking the layers and sealing the cell, while evacuating it down to 1 mbar, the cells were hot pressed for 60 s at 90°C with a pressure of 14.2 bar. Symmetric cells were built up the same way. For this purpose two similar electrodes, either cathodes (Figure 4c) or anodes (Figure 4d) were used. For investigations on the interface to the current collector, cells with a cathode between two current collectors were built up the same way (Figure 4b).

For the cells with a reference electrode, the cell setup as described by Simon et al.[19] was used. These cells were built up in a dry room (relative humidity < 1%). The reference electrode consists of a tungsten wire with a core diameter of 10 µm (99,95%) plated with 3–5 wt% gold (99.99%, Goodfellow Cambridge). For contacting, a nickel tab, which was ultrasonically welded to the wire, was used.

In cells with a reference electrode, the use of electrodes of the same size avoids a geometric asymmetry, which might cause artefacts in the impedance spectrum.[20] The cathode and anode geometric area in these cells is 13.3 cm^2. Each electrode was first pressed with one SPE layer, before building up the complete cell. This cell was pressed one more time. The pressing parameters were the same as listed for the standard full cells above.

Lithiation of the reference electrode was carried out with lithium electrochemically removed from both electrodes. Using a Gamry potentiostat (Reference 600), a current of 1.15 nA was applied between the respective electrode and the reference electrode for 9.6 hours to deposit lithium from the electrodes on the reference electrode. This was done for both electrodes at the same time using two potentiostats. The values correspond to those of Simon et al.[19] for stable reference electrodes.

Characterization.—The chemical composition and electronic structure of the cathode surfaces were analyzed by X ray photoelectron spectroscopy (XPS) at the DAISY-BAT at TU Darmstadt. For this purpose a laboratory analysis unit (VersaProbe from Physical Electronics) was used with a monochromatic Al-Kα source and an incidence angle of 45°. For details of experimental set-up and procedure refer to Hausbrand et al.[29] More details on the PEO evaporation for XPS analysis will be published in a further publication.

For EIS measurements Gamry potentiostats/galvanostats were used in a frequency range from 10 mHz up to 1 MHz (100 kHz for cells with reference electrode) with 10 points per decade in the potentiostatic mode (AC voltage: 10 mV). All measurements were conducted at a temperature of 80°C, which was kept constant by a climatic chamber (Binder/ CTS).

Results and Discussion

Spectral signature of full and symmetric cells.—In Figure 5 the impedance spectrum of a full cell in the initial state is compared to the impedance spectra of a cathode- and a lithium symmetric cell in the Nyquist plot (left) and the Bode plot (right). The impedance data of the symmetric cells are divided by the factor of two to obtain the spectrum of only one electrode. The full cell impedance is a superposition of the cathode and the anode impedances. The semicircle, representing the interface resistances of the full cell is in agreement to the ones obtained from the cathode and the lithium symmetrical cells. For

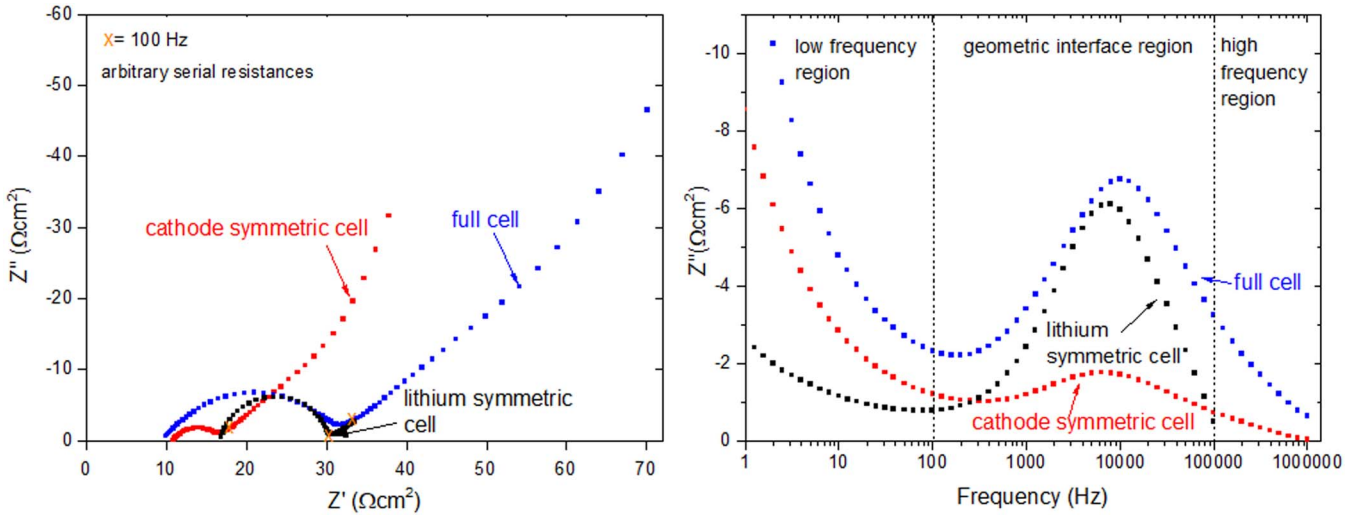

Figure 5. Nyquist plot (left) and Bode plot (right) of EIS spectra of different cell designs. The interface resistance of the full cell (blue) composes of the interface resistance on the lithium side (black) and the one on the cathode side (red). The spectrum of the symmetric cells are shifted on the x-axis for a better illustration. In the Bode plot, the different interface regions are marked.

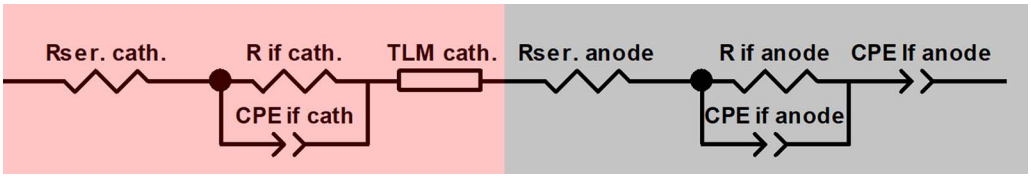

Figure 6. Equivalent circuits for fitting cathode symmetric cells (red) and anode symmetric cells (gray). Due to the porous structure of the composite cathode, the transmission line model is used. For fitting a full cell the complete equivalent circuit can be used.

all cell types, these semicircles arise in the frequencies higher than 100 Hz.

In the Bode plot it can be clearly seen, that the interface resistance to the lithium anode appears in the same frequency range (100 Hz - 100 kHz) as resistances on the cathode side. For this example the characteristic frequencies of both processes are at 7000 Hz. Concerning the cathode and the anode part, there is no preference, which appears at higher frequencies. These similar characteristic frequencies are responsible for the strong overlapping of the semicircles.

The full cell behavior in the region lower than 100 Hz is mainly shaped by the cathode, as seen in Figure 5 and is therefore fitted by the TLM, as described in the introductory section.

The spectra of the symmetrical cells were fitted with the color-coded equivalent circuits displayed in Figure 6. The values obtained by these fits are listed in Table II on the left side, normalized to the respective geometric area (division by the factor of 2 for symmetric cells). Figure 7 shows the full cell spectrum (blue), a simulation obtained from the addition of the symmetric cell fits (red), and the fit curve of the full cell spectrum with the parameters from symmetric cells as initial values (light blue). The full cell spectrum was simulated using the complete equivalent circuit in Figure 6 together with the fit parameters obtained from the symmetric cells. The values of the light blue fitting curve are listed on the right in Table II. The values for the interface resistances only differ by 0.4 Ωcm^2 from the values of the symmetric cells. The relative errors are much higher, however, as the spectrum does not show distinct features for the electrodes. Reliable values for a certain electrode side cannot be achieved in full cells.

Interface resistance between the cathode and the current collector.—The interface resistance between the composite cathode and the aluminum current collector can be determined by using a symmetric cell with the cathode sandwiched between two aluminum foils (Figure 4b). In such a cell, the initial geometric interface resistance, i.e. the diameter of the half-cycle, of 26 $\Omega \cdot cm^2$ is measured (Figure 8). This resistance corresponds to the electronic interface resistance between the current collector and the cathode composite, since there is no other layer in this cell design and no charge transfer is expected to take place. After 12 hours of aging at 80°C, with repeating EIS measurements, an increase of 15 $\Omega \cdot cm^2$ for the impedance of the blocking cell is observed.

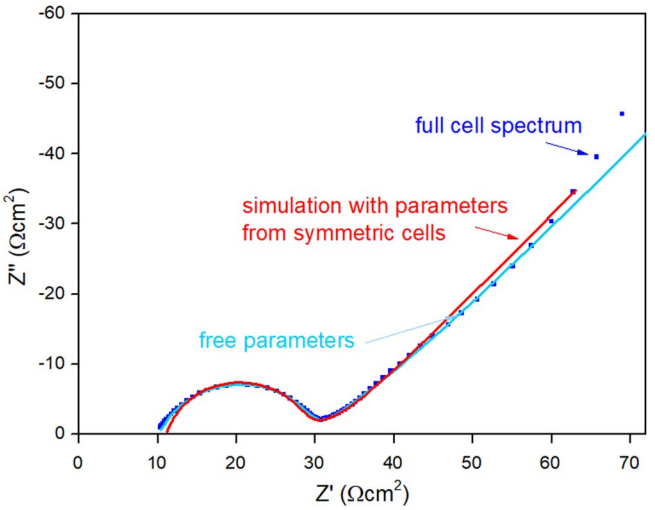

Figure 7. Nyquist plot of a full cell spectrum (blue), fitted with fixed values got from symmetric cells (red) and with free parameters (light blue).

In order to decrease the interface resistance, an aluminum foil coated with a 3 µm electrically conductive carbon layer (SDX, Showa Denko K. K.) was used. Figure 9 shows the spectrum of a cell where C-coated Al was used on both sides of the cathode. Here the interface resistance is $< 0.02\ \Omega \cdot cm^2$, which indicates an electronic path through the cathode connecting the two current collectors. This interface resistance is stable for more than 48 hours at 80°C.

The electronic resistance is resulting from the interface between the current collector and the electronically conductive network of the composite cathode. This network is provided by the carbon conductive additive and the carbon coated LFP. Therefore, a bad contact between these materials must be the reason for this resistance.[21] Such

Table II. Values obtained by the fit of spectra of symmetric cells and of a corresponding full cell spectrum. All the given values are normed on the respective area.

Symmetric cell	Fit parameter	Unit	Fit values from symmetric cell data	Relative error [%]	Fit values from full cell data	Relative error [%]
Cathode	R_{serial}	Ωcm^2	5,65	1,6	9,9	28
	R_{if}	Ωcm^2	3,75	4	4,2	210
	CPE - T_{if}	F/cm^2	$3{,}4 \cdot 10^{-5}$	11	$8{,}5 \cdot 10^{-6}$	61
	CPE- p_{if}	-	0,81	3,9	1	25
	R_{ion}	Ωcm^2	0,11	7,2	0,04	180
	CPE-T_{tlm}	F/cm^2	$3{,}45 \cdot 10^{-4}$	0,97	$2{,}6 \cdot 10^{-4}$	43
	CPE-p_{tlm}	-	0,57	1,4	0,57	13
	n	-	100	-	100	-
Anode	R_{serial}	Ωcm^2	16,43	0,42	-	-
	R_{if}	Ωcm^2	13,0	1,2	12,7	89
	CPE - T_{if}	F/cm^2	$4{,}9 \cdot 10^{-5}$	9,3	$4{,}4 \cdot 10^{-5}$	97
	CPE- p_{if}	-	0,90	1	0,86	14
	CPE – T_{lf}	F/cm^2	$1{,}2 \cdot 10^{-1}$	4,5	$8 \cdot 10^{-2}$	73
	CPE –p_{lf}	-	0,36	6,9	0,21	190

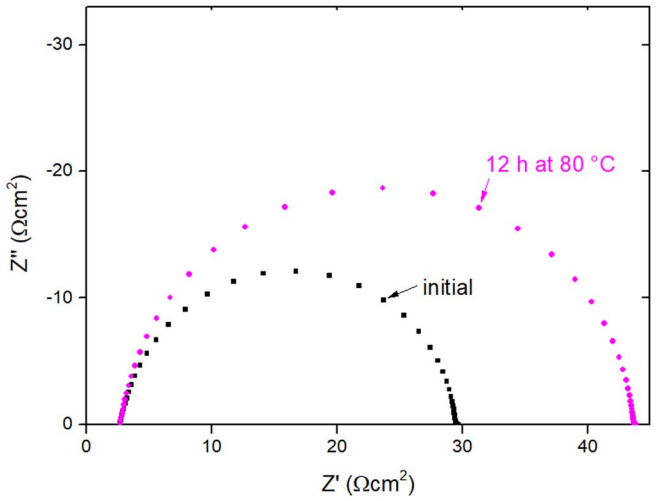

Figure 8. Nyquist plot of a cathode between two plain Al foils (Figure 4b). The spectra of the initial state (black) and after storage for 12 h at 80°C (pink) are displayed. These spectra were measured at 80°C and normalized on the geometric cathode surface area.

a bad contact can occur due to electronic or mechanical reasons. It is not reported that the interface between aluminum and carbon suffers poor electronic properties. Furthermore, the results with the C-coated Al in this work demonstrate that a good electronic contact between carbon and aluminum is possible. Therefore, we presume that the high resistance is due to an insufficient mechanical contact of the two phases, which could be caused by the presence of PEO at the interface. To investigate this further, the chemical compositions of the surfaces of different cathode samples were characterized by XPS. A surface measurement of a standard calendered composite cathode was done. To figure out if the composition on the cathode surface is identical with the one in the bulk material, the cathode was scratched with a scalpel. In addition, a cathode composite that was only pressed and not calandered was measured, to investigate if the difference between the surface and the bulk results from the cathode preparation process.

The C1s spectra of the three examined composite cathodes show two main emission lines (see the three upper spectra in Figure 10), with different intensity ratios. Possible origins of the different contributions

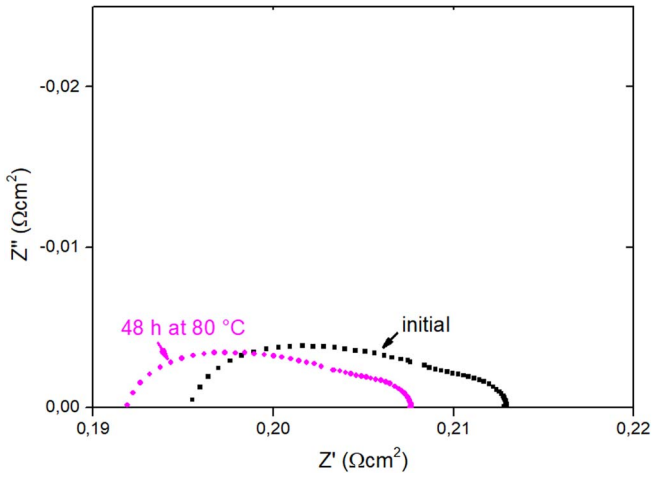

Figure 9. Nyquist plot of a cathode between two carbon coated Al foils (Figure 4b)). The spectrum of the initial state (black) is compared to the one after storage at 80°C for 48 h (pink). The spectra were measured at 80°C and normalized on the geometric cathode surface area. The interface resistance is < 0.02 Ω·cm² and stable during storage at 80°C.

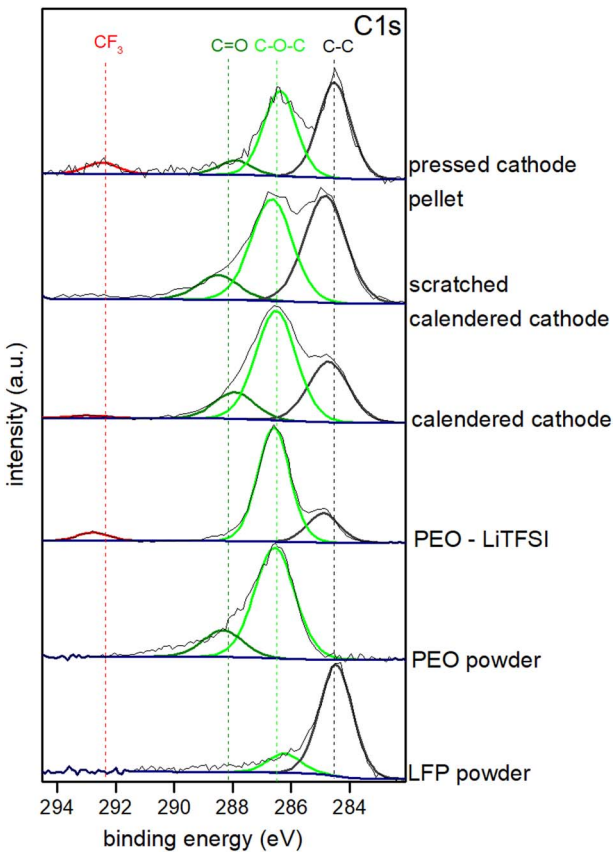

Figure 10. XPS C1s spectra. Curves from the composite cathodes show the emissions of the plain materials, carbon coating on LFP powder (black, 284.5 eV) and PEO - LiTFSI (green, 286.6 eV (PEO) and red 292.9 eV (LiTFSI)). Displayed composite cathodes: pressed cathode pellet, calendered cathode and scratched calendered cathode.

are the carbon species in the PEO, in the carbon black, as well as in the carbon coating on the LFP.

To obtain reference values, measurements of the pure LFP powder, the pure PEO powder as well as of a PEO- LiTFSI membrane were done. In the pure LFP spectrum the main emission line at 284.5 eV is observed, which is attributed to elemental C originating from the carbon coating.[22] A second, smaller emission was detected at 286.2 eV. Such a component is also observed by others[22] for carbon coated LFP and is likely resulting from the preparation process of the commercial C-coated LFP powder by the usage of an organic precursor. Furthermore it might be some adventitious carbon resulting from the ex situ handling of the powder.

The carbon spectrum of the PEO powder, exhibits a main emission line at 286.6 eV which is attributed to the C-O-C carbon species in PEO.[23] This is also the main emission line in the carbon spectrum of the PEO-LiTFSI layer. The minor emission seen at 292.9 eV is corresponding to the carbon species in LiTFSI (CF_3).[23] This layer also exhibits a comparatively high emission for the elemental carbon at 285 eV. The pure PEO powder does not show this component and we presume that it results from the preparation process of the PEO-LiTFSI layer (pressing between two polypropylene foils) which leads to C-C remnants.

In the C1s spectrum of a standard calendered cathode, the content of C contributed to PEO is twice as much as the content of C contributed to elemental carbon. This can be attributed to a high PEO content on the composite cathode surface. Measuring the scratched calendered cathode, the area of the C1s emission for LFP and carbon black is 1.1 times of the emission contributed to PEO.

In comparison to the scratched cathode, an even higher content for LFP and carbon black was detected on the not calendered cathode

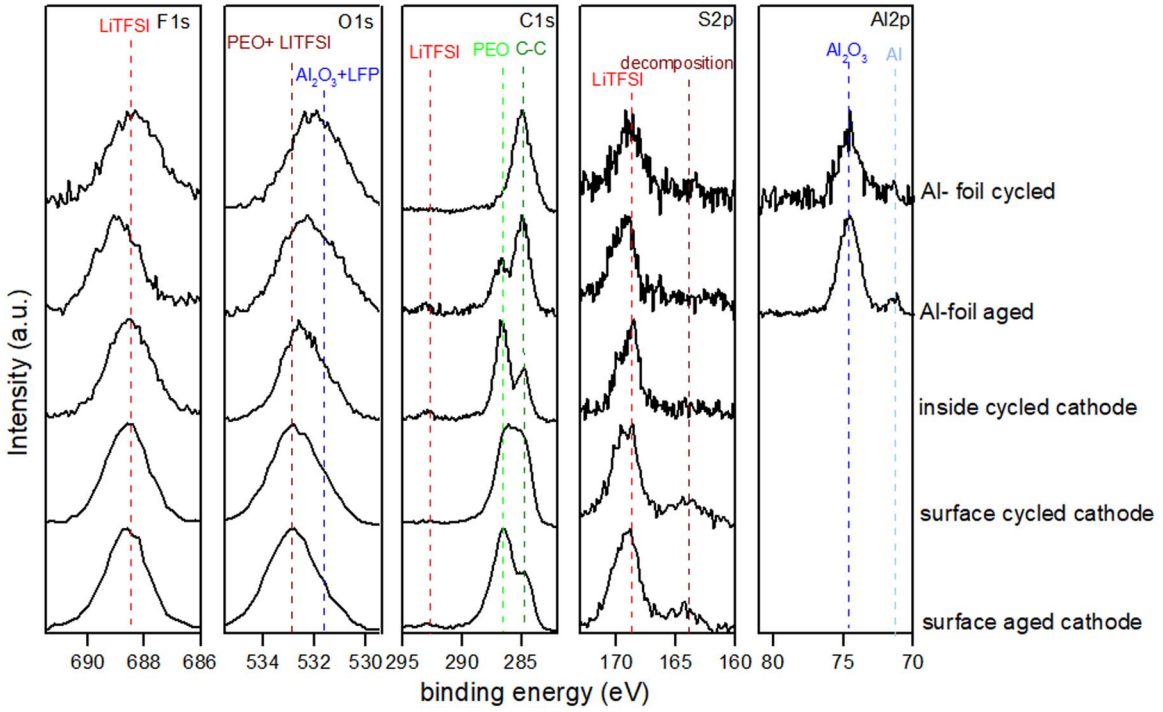

Figure 11. XPS spectra of Al foils, which were removed from different cells, compared to spectra of the opposing composite cathodes. Further explanations can be found in the text. For comparison the spectra of the inside of the cycled cathode is shown. All spectra were calibrated on the C-C emission at 285 eV.

pellet. Possibly, the PEO-rich layer on the surface of a calendered cathode is thicker than the mass removed on the scratched cathode. These results indicate that a change in cathode composition, especially on the surface is induced by the calendering process. Furthermore, they confirm the assumption of a poor mechanical contact between the CAM and carbon additive in the calendered composite cathode and the plain Al current collector.

Osada et al.[24] claim, that the improved contact when using a carbon coated aluminum foil, results from the particulate carbon coating interpenetrating the cathode composite. This statement is in agreement with our results. However, the increase of the interface resistance during storage at 80°C (Figure 8), which is also shown by Osada et al.,[24] is not explained. This increase presumably results from a decreasing electronic contact between the electronic conductive network and the Al. One of the reasons might be a corrosion of the aluminum caused by the $TFSI^-$ anion, since Al has a low standard potential (1.39 V vs. Li) and is only kinetically stable because of its Al_2O_3 passivation layer.[25] This layer is destroyed by the $TFSI^-$ anion as described by Yang et al.[26] forming $Al[N(CF_3SO_2)_2]_3$ (AlTFSI) during this corrosion reaction.

In order to investigate the increase in interface resistance for our system, we conducted XPS measurements. In order to perform these measurements, the Al foils and the composite cathodes were separated and their surfaces, which were formerly in contact and built the interfaces, were analyzed. For carbon coated Al foils, removing from the composite cathodes was impossible. The surfaces of two different uncoated Al foils showing different interface resistances in the cell were analyzed. One was removed from a cathode symmetric cell, which had been aging for three days at 80°C, during which period an increase in interface resistance of 1 $k\Omega \cdot cm^2$ was observed. The second one was cycled for the same duration at 80°C with C/50. Here a large interface impedance increase of 24 $k\Omega \cdot cm^2$ was observed. Table III displays the elemental compositions of the two surfaces. On both samples, Al was detected originating from the current collector. Furthermore, large amounts of carbon and oxygen were observed, as well as small amounts of fluorine and sulfur, indicating that there were residuals of the cathode composite sticking on the Al foil. On both foils, no Fe or P signals were detected. This is in agreement with the assumption that there is mainly PEO- LiTFSI on the surface of the cathode. The amounts detected for F1s and S2p and especially their ratio are comparable for both surfaces. The detected ratio is in agreement with the composition of LiTFSI. More detailed information about the chemical structure can be obtained looking at the binding energies and shapes of the different emissions.

In Figure 11 the XPS spectra measured on both Al-foils as well as the spectra measured at the corresponding composite cathodes are displayed. For comparison the spectra of the inside of the cycled cathode, which was achieved by scratching the cathode, is shown. On the Al-foil that had been removed from the aged cathode symmetric cell, the components in the C1s emission can be attributed to carbon black (285 eV), to PEO (286.6 eV) and to LiTFSI (292.9 eV). The presence of the TFSI anion is also supported by the values of the F1s and $S2p_{3/2}$ emission (688.9 eV and 169.0 eV respectively).[23] The features of the C1s emission are comparable with the ones detected on the aged composite cathode surface but with a lower PEO content. The Al2p spectrum of the foil shows two emission lines. A small one at 72.6 eV, which can be attributed to elemental aluminum and a large one at 74.6 eV, which is assigned to Al_2O_3. The amount of this main signal is in accordance with the O1s emission and the composition for Al_2O_3. Overall, for this sample, the composition and binding energies are well in agreement with an aluminum surface with a thin (native) oxide covered with residual carbon black PEO and LiTFSI salt, originating from the composite cathode. We find no indication of an extensive reaction layer formation, such as the formation of an AlTFSI layer but also cannot rule out the presence of some AlTFSI.[26] Since the Al emission for the AlTFSI would arise at a similar binding energy as the one of Al_2O_3, the existence of a certain amount of AlTFSI is possible.

On the foil removed from the cycled full cell, the C1s spectrum looks very different and no emission allocated to the LiTFSI (292.9 eV) is detectable. The absence of the $TFSI^-$ anion is also supported by different binding energies of the F1s and $S2p_{3/2}$ emissions

Table III. Elemental compositions measured on two different Al foils removed from cells.

Al foil	C1s (at %)	O1s (at %)	F1s (at %)	Al2p (at %)	S2p (at %)
From aged CSC cell	44.3	35.0	5.8	12.9	2.1
From cycled full cell	66.5	21.2	4.0	3.4	1.5

(168.5 eV and 688.4 eV, respectively). Furthermore, the fraction of the emission assigned to PEO is much lower compared to the aged sample. However, there is a remarkable oxygen amount on the Al foil from the cycled cell (see Table III), which is in disagreement with the low PEO signal in the C1s spectrum.

The absence of the CF_3 emission and the slightly shifted F1s and S2p emissions let us assume that there is a reaction occurring on the interface between the plain aluminum foil and the composite cathode during charge. Since there is no signature of TFSI-anions, we conclude that in our case no significant formation of AlTFSI takes place. Possibly, there is an oxygen rich reaction product, which would explain the oxygen excess of 7 at % estimated.

Interface resistance between the composite cathode and the solid polymer electrolyte layer.—The interface resistance between the composite electrode and the SPE can be investigated by cathode symmetric cells. The curves in Figure 12 for cathode symmetric cells with a carbon coated Al current collector show a small but significant interface impedance contribution observed as a semicircle, which does not change during storage at 80°C. As shown before (Figure 9) the contact resistance to the current collector is smaller than 0.02 $\Omega \cdot cm^2$, so there is not significant influence resulting from this interface.

Several explanations can be considered as origin for this interface contribution. One possibility is that this resistance results from the inner cathode interface. Therefore, this resistance would scale with the LFP particle surface inside the cathode. Another possible origin is the geometric interface between the composite cathode and the SPE layer. On this interface, a bad mechanical contact between the layers might cause the resistance.

Fitting this semicircle with an R-CPE element, reveals a corresponding effective capacitance of $(3.0 \pm 0.3) \cdot 10^{-6}$ F/cm^2 based on the geometric cell area. Moreover, we do not expect a contribution of the charge transfer resistance in cathodes in the initial state because of their blocking behavior as described in the introductory section. Nevertheless, it was checked whether the surface area of the LFP particles influences the resistance. Therefore, the area within the cathode is changed by the variation of the cathode thickness. The Nyquist plot

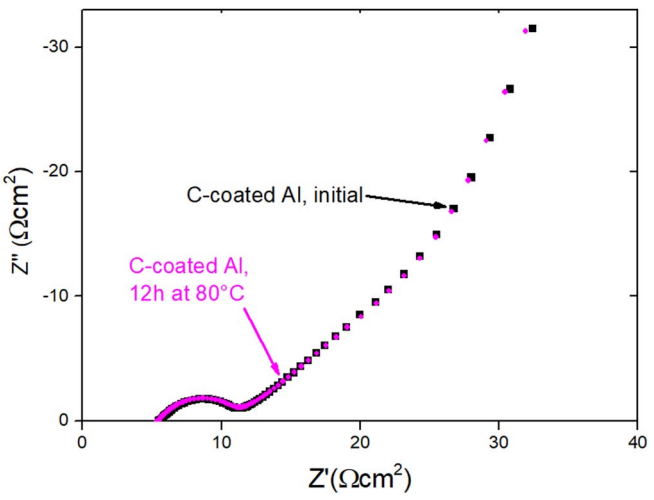

Figure 12. Nyquist plot of spectra of cathode symmetric cells at 80°C, in the initial state (black) and after 12 h at 80°C (pink). The spectra were normalized on the geometric cathode surface area.

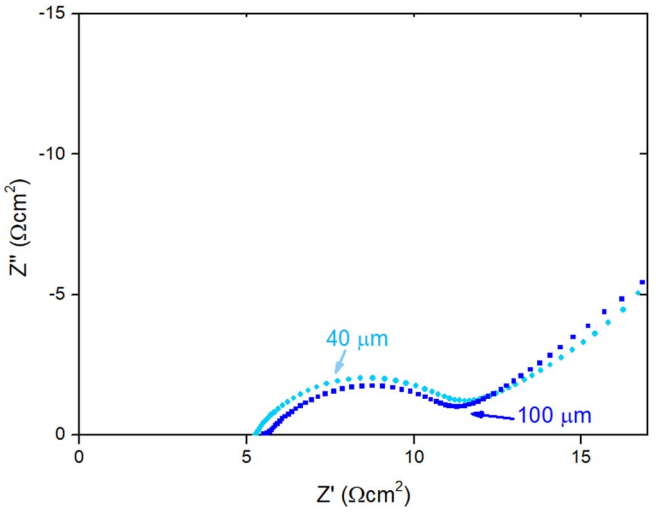

Figure 13. Nyquist plot of spectra of cathode symmetric cells with cathodes of either 40 µm (light blue) or 100 µm thickness (blue) at 80°C.

of the impedance measured on cathode symmetric cells with 40 µm or 100 µm thick cathodes is shown in Figure 13. The value of the interface resistance is (6±1) $\Omega \cdot cm^2$ and therefore not influenced by the cathode internal interface area. As a result, the contribution results presumably from the interface between the cathode and the adjacent SPE layer.

Hanai et al.[4] report an interface resistance between a similar cathode and a PEO-LiTFSI electrolyte separator of 30 $\Omega \cdot cm^2$ at 60°C, comparable in value to 15 $\Omega \cdot cm^2$ at 60°C in our study.

For investigations on the quality of the mechanical contact between the composite cathode and the SPE, one cathode and one polymer electrolyte layer were laminated by a pressing process. The parameters of this process are described in *Experimental*. After this process, gas encapsulations between both layers become visible, as shown in Figure 14a. On sites with a good contact between the black composite cathode and the SPE, the latter one is invisible. The gas encapsulations are identifiable as bright spots.

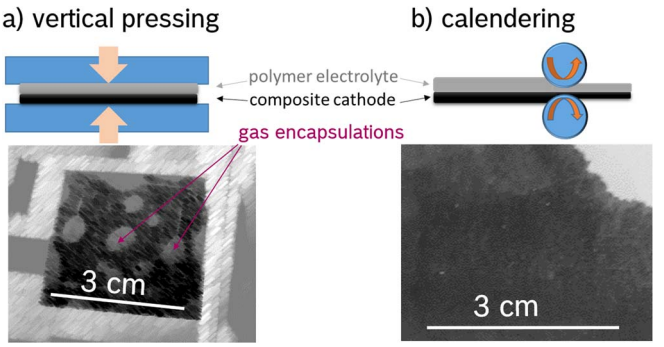

Figure 14. Two ways of providing a contact between the composite cathode (black) and the polymer electrolyte layer (gray). Schematic figures of the processes and pictures of the compounds. After vertical pressing (a) gas encapsulations are visible, after calendering (b), the contact is close without interruption.

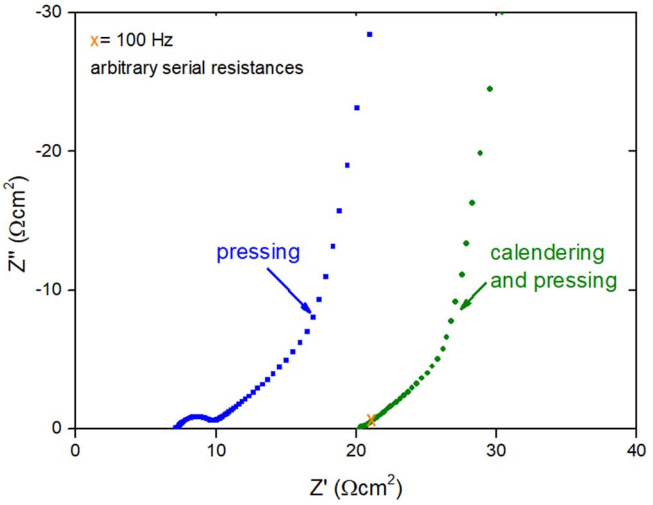

Figure 15. Nyquist plot of EIS spectra of cathode symmetric cells, which were built up by pressing (left, blue) and by calendering and pressing (right, green). For the cell prepared by calendering the bulk resistance is higher since two layers of the SPE are used.

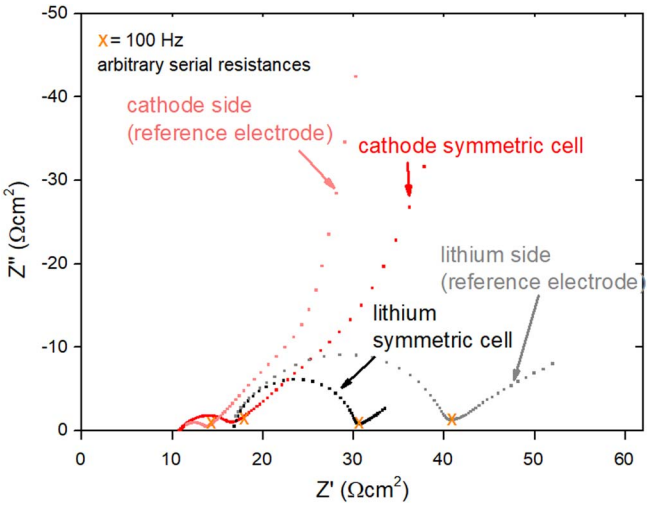

Figure 16. Comparison of the spectra of the anode and the cathode from symmetric cells (black and red) and from a full cell with reference electrode (gray and light red) in the Nyquist plot.

When introducing a calendering step previous to the pressing process, by laminating the cathode film directly to the polymer electrolyte film at a temperature of 100°C, no gas encapsulations are visible (Figure 14b). In this case, two calender rolls exert a force upon the two layers while simultaneously allowing a path for gas to escape.

The impedance data of two cathode symmetric cells assembled according to the two described processes are shown in Figure 15. The interface resistance contribution of the cell assembled by means of the calender process is smaller than 0.2 $\Omega \cdot cm^2$. Thereby, it is reduced significantly compared to cells prepared by vertical pressing.

Additional measurements, which are not shown here, indicate that the interfacial resistance of cathode symmetric cells with a C-coated Al CC is unchanged after ageing for more than 200 h at 80°C regardless of the size of contact resistance to the SPE.

Charge transfer resistance between the CAM and the catholyte.—To characterize the cathode impedance at different SOC, a reference electrode design was applied. By characterizing a full cell, the reference electrode enables the separation of the spectrum in a cathode and an anode part.

In Figure 16 the anode and the cathode half cell spectra of a full cell in the initial state with a reference electrode are compared to the spectra of cathode and lithium symmetric cells. For these cells, C-coated Al current collectors were used, but no calendering was done for improving the contact between the composite cathode and the SPE. Since the cells with reference electrode are assembled in the dry room and the calendering step is also done there, the time, the components are exposed to the humidity is increased by calendering, which causes an even higher interface resistance to the lithium anode. The 10^4 times higher H_2O content (1% in the dry room compared to <1 ppm in the glove box) reacts with the Li surface causing presumably Li_2O which results in a higher resistance on the interface.[12]

The spectra obtained by the use of a reference electrode are comparable to the ones obtained from symmetric cells concerning their frequency dependent shape. However, the Nyquist plot (Figure 16) visualizes that the geometric interface resistances are differing. The higher Li/ SPE interface resistance in the anode spectrum of the cell with a reference electrode is resulting most probably from the fact that the assembly of these cells was done in a dry room, while the lithium symmetric cells with a smaller interface resistance were assembled in a glove box.

The geometric interface resistance on the cathode side of the full cell with the reference electrode is smaller than in the cathode symmetric cell. This means, that the mechanic contact between the composite cathode and the SPE is better. Presumably, the difference results from the variation in the pressing process. As described in *Experimental*, the cathode and the SPE were pressed separately before pressing the complete cell, which is not the case in symmetric cells. This might cause a lower interface resistance between the cathode and the SPE.

In Figure 17, cathode spectra from a full cell with reference electrode at different SOC are shown. These spectra were achieved by charging and discharging the cell with a charging rate of C/10 (0.15 mA/cm²) in one-hour steps. Before conducting the EIS measurements, the cell was allowed to equilibrate during an OCV step of one hour.

The contact resistance between the composite cathode and the SPE, represented by the semicircle at frequencies higher than 100 Hz, does not change with the SOC. In the frequency region lower than 100 Hz the spectra differ depending on the SOC. This is the part of the spectra, which is modelled by the transmission line model, discussed in the introductory section.

At the different SOC between the fully charged and the fully discharged state R_{CT} was determined in the frequency region between 1 Hz and 100 Hz. Two assumptions were made for this determination. First, the electronic resistance (R_{el}) is assumed much lower than the

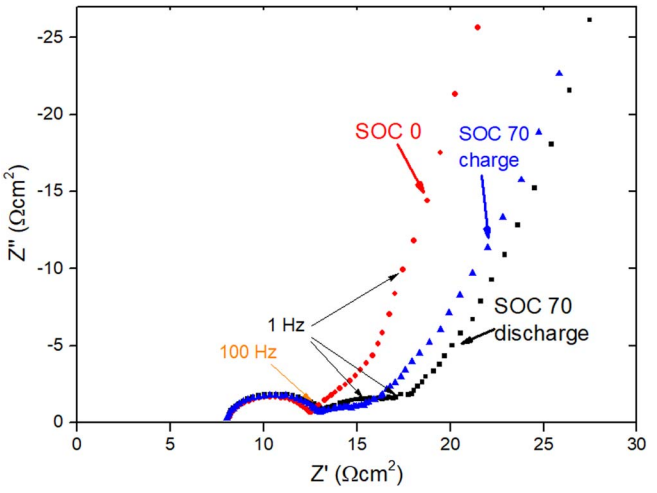

Figure 17. Nyquist plot of the cathode impedance obtained from a full cell with reference electrode. Spectra in the discharged state SOC 0 (red) and at SOC 70 achieved during charge (blue) as well as during discharge (black).

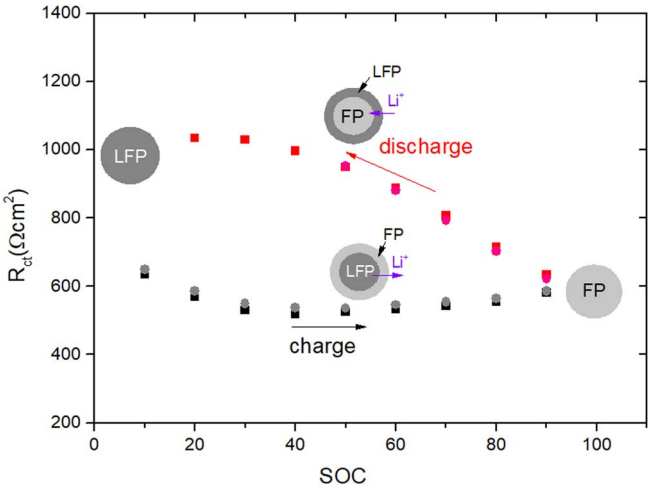

Figure 18. SOC dependence of the charge transfer resistance. Two cycles of one full cell are plotted. An assumption of the structure of the LFP particles at different states is displayed.

ionic one, therefore it was neglected. Secondly, the ionic resistance R_{ion} through the cathode, particularly through the catholyte phase is not affected by the SOC. This resistance is determined from impedance spectra of cells in the discharged state, since here it is not superimposed by R_{CT}. For the modelling of spectra at other SOC the value for R_{ion}, determined in the discharged state was kept constant.

Figure 18 shows the fit values for R_{ct} as a function of SOC. The resistances are based on the surface area of the AM particles in the cathode layer. Clearly, the resistance is higher for the discharge process than for the charge process. For the charge process, the resistance is between 520 and 630 Ωcm.[2] For the discharge, the data indicate that the resistance strongly increases during the process from 620 Ωcm^2 at SOC 90 to 1030 Ωcm^2 at SOC 20. Therefore, the R_{CT} is dependent on the SOC as well as on the direction how the SOC is achieved.

Principally, such changes in the interface resistance may be caused by changes in the near surface region of the active material, by a modified interfacial region in the electrolyte, or by the formation of an interlayer. In order to investigate the interface formation, XPS measurements on the interfaces between LFP/FP and PEO and LFP and LiTFSI were done. In Figure 19 photoemission spectra of LFP powder and delithiated LFP powder ($FePO_4$, FP) are shown in the initial state and after the deposition of a thin PEO layer. PEO was deposited by an evaporation process on the pressed powder.[30]

The C1s and O1s spectra were fitted with two components for both the C1s and the O1s emission in the initial state. In the C1s spectra, the main component is the carbon coating on the particles at 284.4 eV and small components at higher binding energies, possibly resulting from partly oxidized carbon residuals from the preparation process. In the O1s spectrum there are two components resulting from the $(Li)FePO_4$ structure. While the spectra of the LFP powder show the typical behavior of Fe^{2+}, the ones of the FP powder exhibit the characteristics of a Fe^{3+} emission.[22] The Fe2p spectra are not changing during the PEO evaporation.

Fitting the O1s and C1s spectra after the PEO evaporation additional components at 286.7 eV/ 286.4 eV (C1s LFP/ FP) and at 532.6 eV/ 532.3 eV (O1s LFP/ FP) appeared. These emissions are assigned to PEO.[23] Therefore all components could be assigned to either PEO or LFP/FP. Since there are no additional components appearing during the PEO evaporation, it can be assumed that there is no reaction product between LFP and PEO neither in the lithiated nor in the delithiated state. In a further experiment, an evaporation of LiTFSI on a planar, sputtered LFP layer was characterized. Here also no reaction product

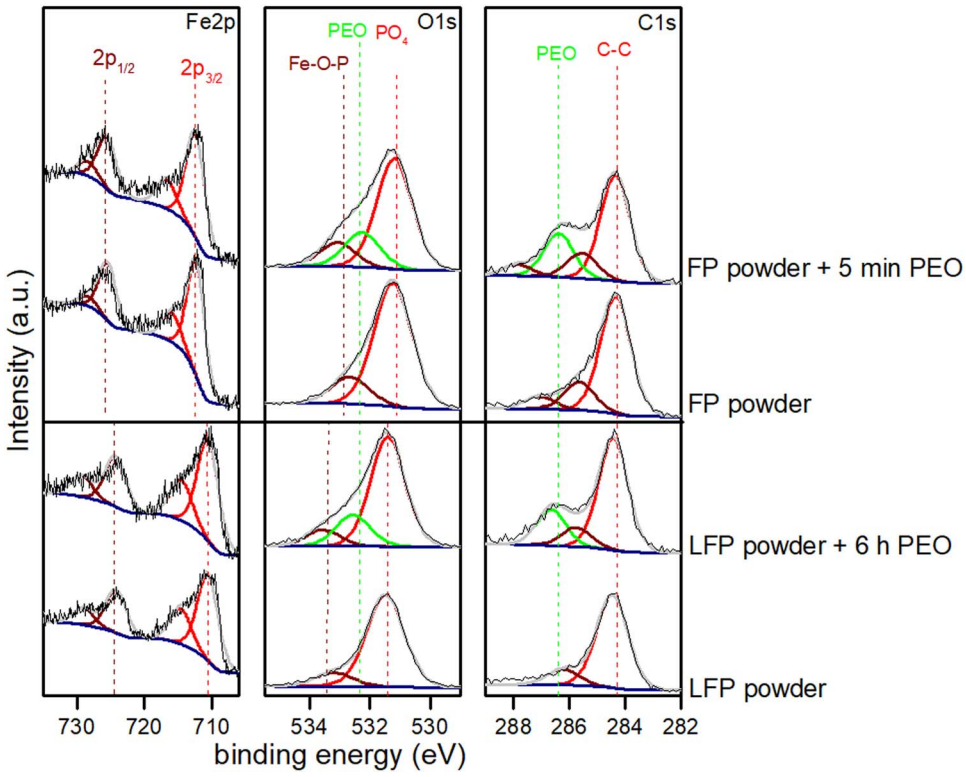

Figure 19. Fe2p, O1s and C1s XP spectra of LFP and FP powder in the initial state and after PEO deposition. FP powder was produced by chemical delithiation of the LFP powder. The PEO deposition was done in situ in an UHV system. The high variation in deposition times on the both powders is resulting from a variation in the surface roughness of the respective pellets. These spectra were chosen to have a comparable amount of detected PEO. For the fitting procedure the O1s and C1s spectra after the PEO evaporation, the components, which were existing in the initial state, were kept constant.

was detected. These experiments demonstrate that reaction at the interfaces is unlikely, i.e. that no reaction layer is affecting the charge transfer resistance.

This indicates that the reason for the variation of the charge transfer resistance results from the particles. It could be a change in the near surface region or an inner particle phenomenon.

The higher resistance in case of the discharge process may be explained by the core shell model proposed by Padhi et al.[14] According this model, the near-surface region of the particle is in a fully lithiated state during the discharge process, while it is in delithiated state during the charge process. Accordingly, the interface resistance is higher during the discharge process since virtually all Li^+-sites are occupied.

To explain the increase in resistance during the discharge process, the layer of LFP formed on the FP particle, could be taken into account. The thickness of this layer grows with the ongoing discharge process. However, the charge transfer takes place only on the surface of the LFP particle on the interface to the catholyte, so the thickness of the several layers inside the particle should actually not influence the R_{CT}.

Concerning this fact, the mobility of the charge carriers inside the LFP particles has to be taken into account. According to Mao et al.[27] the lithium-ion diffusion coefficient in $LiFePO_4$ is lower than in $FePO_4$. Applying this to the core shell model, this fits the measured resistance behavior.

With the TLM used in this work, no distinct statement can be made, concerning the increasing resistance during the discharge process. A modified TLM has to be implemented, with an additional resistance element, in series to all R_{CT}-CPE_{CT} elements, describing the conductivity inside the particles.

Braun et al.[28] introduces a finite-space Warburg element for the solid-state diffusion inside the CAM particles in series to all R_{CT}-CPE_{CT} elements. However, since the solid-state diffusion is generally a very slow process, it is expected to appear at very low frequencies and is therefore not influencing the frequency region, the R_{CT} was fitted. However, since our active material particles are relatively small, the diffusion might be faster than expected, which would explain the appearance at higher frequencies.

From our model, we can conclude, that the core shell model might describe our results the best. However, the contributions of the solid-state diffusion and the charge transfer, to this resistance are not clarified yet.

Summary

In this work, the resistances of different interfaces in cells with LFP/PEO composite cathodes were characterized by electrochemical impedance spectroscopy. Information about the several resistances was gained by the implementation of different cell designs. Significant reductions of the interface resistances to the aluminum current collector, as well as to the polymer electrolyte separator were achieved by a carbon coated current collector and a better contact was achieved by a calendering step.

For the characterization of the charge transfer resistance, cathode spectra at different SOC were recorded by the implementation of a three-electrode setup. This setup enabled the separation of the impedance spectra of the two electrodes in a full cell.

These cathode spectra were fitted by the transmission line model. The obtained values for the charge transfer resistance show a high dependence on the SOC as well as on the charging direction. This result is in accordance with the core shell model for the delithiation and lithiation mechanism of the LFP particles. To clarify the reason for the increasing resistance during the discharge process of a particle, further investigations have to be pursued. One could be the implementation of a modified TLM, considering the mobility inside the CAM particle.

Acknowledgments

Thanks to Jean Philippe Beaupain and Nils Baumgarten, who contributed to this work during their research internships at Robert Bosch GmbH, to Fabian Simon for his help building up the reference electrode cells and to Conrad Guhl for helpful discussions.

ORCID

Verena Wurster https://orcid.org/0000-0002-4131-1054
Wolfram Jaegermann https://orcid.org/0000-0003-3677-4481
René Hausbrand https://orcid.org/0000-0003-4601-4769

References

1. K. Takada, in *AIP Conference Proceedings* (2016).
2. Y. Xia, K. Tatsumi, T. Fujieda, P. P. Prosini, and T. Sakai, *J. Electrochem. Soc.*, **147**(6), 2050 (2000).
3. B. Scrosati, *J. Power Sources*, **100**(1–2), 93 (2001).
4. K. Hanai, M. Ueno, N. Imanishi, A. Hirano, O. Yamamoto, and Y. Takeda, *J. Power Sources*, **196**(16), 6756 (2011).
5. M. Gauthier, P. Ricoux, M. B. Armand, D. Fauteux, J. M. Chabagno, D. Deroo, G. Vassort, D. Muller, A. Bélanger, P. Rigaud, and M. Duval, *J. Electrochem. Soc.*, **132**(6), 1333 (1985).
6. J. Euler and W. Nonnenmacher, *Electrochim. Acta*, **2**(4), 268 (1960).
7. J. Landesfeind, D. Pritzl, and H. A. Gasteiger, *J. Electrochem. Soc.*, A1773 (2017).
8. J. T. S. Irvine, A. R. West, E. Amano, A. Huanosta, and R. Valenzuela, *Solid State Ionics*, **40–41**, 220 (1990).
9. N. Ogihara, S. Kawauchi, C. Okuda, Y. Itou, Y. Takeuchi, and Y. Ukyo, *J. Electrochem. Soc.*, **159**(7), A1034 (2012).
10. C. H. Chen, J. Liu, and K. Amine, *J. Power Sources*, **96**(2), 321 (2001).
11. R. Petibon, C. P. Aiken, N. N. Sinha, J. C. Burns, H. Ye, C. M. VanElzen, G. Jain, S. Trussler, and J. R. Dahn, *J. Electrochem. Soc.*, **160**(1), (2013).
12. R. Bouchet, S. Lascaud, and M. Rosso, *J. Electrochem. Soc.*, **150**(10), A1385 (2003).
13. A. Bünting, S. Uhlenbruck, C. Dellen, M. Finsterbusch, C.-L. Tsai, D. Sebold, H. P. Buchkremer, and R. Vaßen, *J. Power Sources*, **281**, 326 (2015).
14. A. K. Padhi, K. S. Nanjundaswamy, and J. B. Goodenough, *J. Electrochem. Soc.*, **144**, 1188 (1997).
15. R. Malik, A. Abdellahi, and G. Ceder, *J. Electrochem. Soc.*, **160**, A3179 (2013).
16. K. Hanai, K. Kusagawa, M. Ueno, T. Kobayashi, N. Imanishi, A. Hirano, Y. Takeda, and O. Yamamoto, *J. Power Sources*, **195**(9), 2956 (2010).
17. H. Graebe, A. Netz, S. Baesch, V. Haerdtner, and A. Kwade, *ECS Trans.*, **77**(11), 393 (2017).
18. K. Hanai, T. Maruyama, N. Imanishi, A. Hirano, Y. Takeda, and O. Yamamoto, *J. Power Sources*, **178**(2), 789 (2008).
19. F. J. Simon, L. Blume, M. Hanauer, U. Sauter, and J. Janek, *J. Electrochem.Soc.*, **165**(7), A1363 (2018).
20. M. Ender, A. Weber, and E. Ivers-Tiffée, *J. Electrochem. Soc.*, **159**(2), A128 (2012).
21. M. Gaberscek, J. Moskon, B. Erjavec, R. Dominko, and J. Jamnik, *Electrochemical and Solid-State Letters*, **11**(10), A170 (2008).
22. S. J. Rajoba, L. D. Jadhav, P. S. Patil, D. K. Tyagi, S. Varma, and B. N. Wani, *J. Electron. Mater.*, **46**(3), 1683 (2017).
23. C. Xu, B. Sun, T. Gustafsson, K. Edström, D. Brandell, and M. Hahlin, *J. Mater. Chem. A*, **2**(20), 7256 (2014).
24. I. Osada, J. von Zamory, E. Paillard, and S. Passerini, *J. Power Sources*, **271**, 334 (2014).
25. R. Korthauer, *Handbuch Lithium-Ionen-Batterien*, Berlin, Springer Vieweg (2013).
26. H. Yang, K. Kwon, T. M. Devine, and J. W. Evans, *J. Electrochem. Soc.*, **147**(12), 4399 (2000).
27. Z.-Y. Mao, Y.-P. Sun, and K. Scott, *J. Electroanal. Chem.*, **766**, 107 (2016).
28. P. Braun, C. Uhlmann, M. Weiss, A. Weber, and E. Ivers-Tiffée, *J. Power Sources*, **393**, 119 (2018).
29. R. Hausbrand, G. Cherkashinin, M. Fingerle, and W. Jaegermann, *J. Electron Spectrosc. Relat. Phenom.*, **211**, 65 (2017).